

# Accelerated Multi-Modal MR Imaging with Transformers

Chun-Mei Feng, Yunlu Yan, Geng Chen, Huazhu Fu, *Senior Member, IEEE*,  
Yong Xu, *Senior Member, IEEE*, and Ling Shao, *Fellow, IEEE*

**Abstract**— Accelerated multi-modal magnetic resonance (MR) imaging is a new and effective solution for fast MR imaging, providing superior performance in restoring the target modality from its undersampled counterpart with guidance from an auxiliary modality. However, existing works simply combine the auxiliary modality as prior information, lacking in-depth investigations on the potential mechanisms for fusing different modalities. Further, they usually rely on the convolutional neural networks (CNNs), which is limited by the intrinsic locality in capturing the long-distance dependency. To this end, we propose a multi-modal transformer (MTrans), which is capable of transferring multi-scale features from the target modality to the auxiliary modality, for accelerated MR imaging. To capture deep multi-modal information, our MTrans utilizes an improved multi-head attention mechanism, named cross attention module, which absorbs features from the auxiliary modality that contribute to the target modality. Our framework provides three appealing benefits: (i) Our MTrans is the first attempt at using improved transformers for multi-modal MR imaging, affording more global information compared with existing CNN-based methods. (ii) A new cross attention module is proposed to exploit the useful information in each modality at different scales. It affords both distinct structural information and subtle pixel-level information, which supplement the target modality effectively. (iii) We evaluate MTrans with various accelerated multi-modal MR imaging tasks, e.g., MR image reconstruction and super-resolution, where MTrans outperforms state-of-the-art methods on fastMRI and real-world clinical datasets.

**Index Terms**— MR imaging, multi-modal, reconstruction, super-resolution.

## I. INTRODUCTION

Magnetic resonance (MR) imaging is rapidly becoming the dominant technique for image-guided adaptive radiotherapy because it offers better soft tissue contrast than computed tomography (CT), while avoiding radiation exposure. However, due to the physical nature of the MR imaging procedure, the scanning time can take up to tens of minutes long, which seriously affects the patient experience and leads to high

C.-M. Feng, Y. Yan and Y. Xu are with the Shenzhen Key Laboratory of Visual Object Detection and Recognition, Harbin Institute of Technology (Shenzhen), 518055, China. (Email: strawberry.feng0304@gmail.com; yongxu@ymail.com).

G. Chen and H. Fu and L. Shao are with the Inception Institute of Artificial Intelligence, Abu Dhabi, UAE. (Email: {hzfu, ling.shao}@ieee.org).

Corresponding author: Huazhu Fu and Yong Xu.

C.-M. Feng and Y. Yan are contributed equally to this work. This work was done during the internship of C.-M. Feng at Inception Institute of Artificial Intelligence.

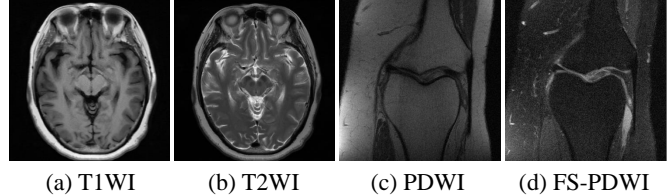


**Fig. 1:** Examples of four different modalities. Images (a) and (b) are a T1WI and T2WI from the same subject of a real-world clinical dataset. Images (c) and (d) are a PDWI and FS-PDWI from the same subject of fastMRI. Different modalities from the same subject have inter-modality consistent structure.

costs. Therefore, accelerated MR imaging has become a hot research topic, where reconstructing images from undersampled  $k$ -space measurements is a standard strategy. However, the aliasing artifacts caused by insufficient sampling often affect the clinical diagnosis. Therefore, the recovery of high-quality images from undersampled  $k$ -space measurements is the ultimate goal when accelerating MR imaging. Currently, mainstream methods for this include MR image reconstruction and super-resolution (SR). The former aims to remove the aliasing artifacts caused by undersampling [1]–[4], while the latter enhances the image resolution [5]–[7].

According to different acquisition parameters, the scanner provides MR images with different modalities. For the same subject, these modalities often have inter-modality consistent information and modality-specific information [8]. In addition, the acquisition procedures of the different modalities vary. For example, T1 and T2 weighted images (T1WIs and T2WIs), as well as proton density and fat-suppressed proton density weighted images (PDWIs and FS-PDWIs), are two pairs of images with complementary structures. As shown in Fig. 1, (a) and (b) are a pair of T1W and T2W brain MR images from the same subject of a real-world clinical dataset, where (a) provides morphological and structural information, and (b) shows edema and inflammation. Following [9], we filter out pairs of PDW and FS-PDW images from fastMRI (currently the largest available database for raw MR images), as shown in Fig. 1 (c) and (d). PDWIs provide structural information for articular cartilage, while FS-PDWIs can inhibit fat signals and highlight the structural contrast between cartilage ligaments and other tissues [10]. Due to the physical characteristics of the MR imaging, T1WIs are more easily acquired than T2WIs since they require a shorter repetition time (TR) and

echo time (TE). Similarly, PDWIs require a shorter scan time than FS-PDWIs. Therefore, we can use relatively easy-to-obtain modalities as supplementary information to guide and accelerate target modalities that are acquired with slower imaging speeds. Motivated by this, the joint learning of multi-modal images has provided a new framework for accelerated MR imaging.

Various traditional techniques, such as compressed sensing (CS), Bayesian learning, dictionary learning, and graph representation theory, have been employed to accelerate multi-modal MR imaging [11]–[13]. More recently, deep learning has become the focus of multi-modal MR imaging studies [14], [15]. For example, Salman *et al.* added an auxiliary modality as prior information into the generator of a generative adversarial network (GAN) [15]. Lyu *et al.* concatenated the two modalities at the feature level of smaller size [16]. However, most of these methods simply downsample the magnitude images to simulate the acquisition of undersampled or low-resolution (LR) MR image scans, implying that their effectiveness for fast multi-modal MR image remains to be verified [14], [15]. In addition, different MR image modalities have modality-specific appearances under different intensity distributions. *Thus, how to effectively fuse the two modalities is an inherent problem in multi-modal MR imaging, which needs to be resolved.* On the other hand, convolutional neural networks (CNNs) struggle to fully capture global knowledge due to its intrinsic locality of convolution operations, while transformers can learn global information by modeling long-range dependency. Benefiting from this, transformers have recently achieved state-of-the-art performance on a variety of computer vision tasks [17]. For example, the Vision Transformer (ViT) divides images into small patches and uses a transformer to model the correlation between them as sequences, achieving satisfactory results in image classification [18]. The Detection Transformer (DETR) formulates target detection as an ensemble prediction task with the help of a transformer [19]. Transformers have also been used in medical imaging tasks. For example, transformers incorporated into UNet have been employed for medical image segmentation [20], [21].

Although recent works have demonstrated the advantages of transformers in vision tasks, *the potential benefits of transformers for multi-modal MR imaging remain to be verified.* To this end, in this work, we investigate how to design a powerful transformer model capable of learning multi-modal representations to enhance various accelerated MR imaging tasks. We propose a multi-modal transformer (MTrans) to fuse the informative features from MR imaging scans of different modalities based on a multi-modal transformer. Our method utilizes multi-scale patches generated by the two-branch transformer to represent different modalities, and merges them to complement each other. Another key contribution of our work is to develop a feature fusion strategy for multi-modal MR imaging transformers, which, to the best of our knowledge, has not yet been investigated. This is achieved with our effective multi-modal cross attention modules, each of which takes the features from the other branch as keys and values, employing them for effectively querying, and obtain useful information from the other modality. In addition, the multi-scale patches

for two branches can capture distinct structural information as well as subtle pixel-level information. Overall, the main contributions of our work are as follows:

- We propose a novel transformer architecture, named MTrans, to accelerate multi-modal MR imaging. Our work is the first attempt at using transformers for this task, which is able to capture rich global knowledge compared with the existing CNN-based methods<sup>1</sup>.
- We also introduce a cross attention module to effectively extract useful information in each branch, and then combine the features from multiple scales to afford both distinct structural information and subtle pixel-level information.
- We evaluate our method on two fast MR imaging tasks, *e.g.*, image reconstruction and SR, on fastMRI and a raw MR image datasets. The results show that our method is superior to other multi-modal MR imaging models in both qualitative and quantitative evaluation.

## II. RELATED WORK

### A. Deep Learning for Accelerated MR Imaging

Image reconstruction and SR techniques can improve image quality without changing the MR image acquisition hardware, therefore they have been widely used for accelerated MR imaging. Traditional technologies such as CS [22], low rank [23]–[26], and dictionary learning [27], [28] have made progress in this task. More recently, deep learning has been widely used. Compared with traditional algorithms, which rely on the prior information of data, deep learning can make full use of the inherent characteristics of images contained in a large amount of training data [29]. For example, Yang *et al.* proposed a model-based unrolling method by applying the alternating direction method of multipliers (ADMM) algorithm to optimize the architecture [30]. MoDL then introduced another model-based unrolling method combining prior regularization [3]. More recently, end-to-end approaches have shown advantages in accelerated MR imaging [31]. Jin *et al.* applied UNet to capture spatial information for inverse problems related to MR imaging [32]. A 3D CNN with a residual architecture was used to generate high-quality MR image scans of knees in [6]. Chen *et al.* recovered high-quality image details from a densely connected SR network [33]. Zhu *et al.* effectively estimated the mappings by manifold approximation (AUTOMAP) for MR image reconstruction [34]. Dongwook *et al.* [35] trained the magnitude and phase of MR image data separately and fused them to generate the output image. To address the shortcomings of CNNs in calculating complex MR image numbers, we recently proposed Dual-OctConv to deal with complex components at various spatial frequencies for accelerated parallel MR imaging [36], [37]. This method not only considers the computational relationship between the real and imaginary parts, but also captures the characteristics of different spatial frequencies. Finally, inspired by the prominent use of GANs in natural image synthesis, many works have used GANs with an adversarial and perceptual loss to generate high-quality MR images [38]–[41]. The

<sup>1</sup>Code is available at: <https://github.com/chunmeifeng/MTrans>.

data consistency layer plays an important role in MR imaging to keep the reconstructed image consistent with the original image in the  $k$ -space [42], [43]. Additionally, hybrid domain learning schemes have been used to recover data from both the  $k$ -space and image domain [44]. However, these methods are all based on a single-modal CNN architecture. In contrast, our method is a multi-modal fusion approach based on the transformer architecture.

### B. Multi-Modal Medical Image Representation

Multi-modal fusion allows multiple modalities to be combined in a new space by taking advantage of complementarities between data, which is more robust than using any single modality as input. Recently, multi-modal technology has also been used widely in medical imaging [8], [14]–[16], [45]. For example, a hybrid-fusion network was designed for multi-modal MR image synthesis [46]. For accelerated MR imaging, Xiang and Dar *et al.* simply concatenated the two modalities as input to guide the reconstruction and SR of the target modality [8], [15]. Sun *et al.* sent the different modalities into the network together to restore them simultaneously [14]. For the MR image SR task, Lyu *et al.* concatenated the two modalities on the features of smaller size [16], while Zheng *et al.* concatenated them on the original image size [45]. However, these existing multi-modal methods simply add the auxiliary modality as prior information for the target modality to improve the image quality; fusing the two modalities has not been explored [8], [14]–[16]. In addition, most previous methods simply downsample the magnitude images to simulate the acquisition of undersampled or LR MR image scans. However, MR imaging acceleration should be done using real  $k$ -space data. Therefore, the effectiveness of fast multi-modal MR imaging remains to be verified.

## III. OVERVIEW OF ACCELERATED MR IMAGING

Let  $\mathbf{y}$  represent the complex-valued, fully sampled  $k$ -space acquired from the MR image scanner. We can obtain the corresponding fully sampled image by  $\mathbf{x} = \mathcal{F}^{-1}(\mathbf{y})$ , where  $\mathcal{F}^{-1}$  is an inverse 2D fast Fourier transform (FFT). In clinical practice, as only the magnitude images are visible, hospitals usually retain these for medical diagnosis. However, in this work, all data (*e.g.*, the zero-filled image for reconstruction and LR image for SR) are obtained from real MR image  $k$ -space data to explore the effectiveness of accelerated MR imaging. This is an important point that has been neglected by current fast multi-modal MR imaging methods. In this work, we consider two kinds of accelerate MR imaging techniques, including (i) reconstructing a clear image from an image corrupted by aliasing artifacts (undersampled image) and (ii) restoring an SR image from a degraded image.

### A. Accelerating MR Imaging by Reconstruction

Let  $M$  be the binary mask operator. We can obtain the undersampled  $k$ -space data by  $\hat{\mathbf{y}} = M \odot \mathbf{y}$ , where  $\odot$  denotes element-wise multiplication. In this work, we use random masks with  $6 \times$  acceleration to select a subset of the  $k$ -space

points. Accordingly, the zero-filled image can be obtained by  $\hat{\mathbf{x}} = \mathcal{F}^{-1}(\hat{\mathbf{y}})$ . Different from current efforts, which address the task by directly restoring  $\mathbf{x}'$  from  $\hat{\mathbf{y}}$  or  $\hat{\mathbf{x}}$ , we introduce an image from an additional modality with the same structural information to restore the target modality.

### B. Accelerating MR Imaging by Super-Resolution

The training phases of previous MR image SR methods usually add Gaussian blurs to the downsampled amplitude image to obtain an LR image [47]. However, simply reducing the image size in the image domain contradicts the actual MR image acquisition process. Following [5], we first truncate the outer part of the fully sampled  $k$ -space  $\mathbf{y}$  by a desired factor to degrade the resolution, and then apply  $\mathcal{F}$  to obtain the degraded LR image  $\tilde{\mathbf{x}}$ . This better mimics the real image acquisition process and avoids checkerboard artifacts.

## IV. PROPOSED MTRANS ARCHITECTURE

In our MTrans, the image patches are processed into a series of linearly embedded sequences to create a dual-branch structure. As shown in fig2, the overall architecture of our MTrans consists of three components. Specifically, two heads are employed for extracting modality-specific features of different scales from the multi-modal input images (*e.g.*, a fully sampled auxiliary modality image of large size with target zero-filling or LR image of small size); a multi-modal transformer is established for aggregating the different modalities, where the module uses the feature of the current branch as the query to exchange information with the other branch; and two tails are used for mapping the features into restored images. Note that, the inputs from different modalities are divided into image patches of different sizes. This enables structural features to be extracted, while also capturing subtle pixel-level information to supplement the target modality. The main goal of the multi-modal transformer is to integrate multi-modal images at different scales. We will next introduce our architecture in detail.

### A. Heads

To extract modality-specific features from different modalities, two branches with different heads (*e.g.*,  $\text{Head}_{aux}$  for the auxiliary modality and  $\text{Head}_{tar}$  for the target modality) are used, each of which consists of three  $3 \times 3$  convolutional layers. The ground truth of the auxiliary modality  $\mathbf{x}_{aux} \in \mathbb{R}^{1 \times H \times W}$  is sent to  $\text{Head}_{aux}$  to generate an auxiliary feature map  $\mathbf{F}_{aux} \in \mathbb{R}^{C \times H \times W}$ , where  $C$  is the number of channels, and  $H$  and  $W$  are the height and weight of the feature maps. For the MR image reconstruction task, we send the zero-filled image  $\hat{\mathbf{x}}_{tar}$  of the target modality to  $\text{Head}_{tar}$  to generate a feature map  $\mathbf{F}_{tar} \in \mathbb{R}^{C \times H \times W}$ , while the LR image  $\tilde{\mathbf{x}}_{tar}$  is used to generate a feature map  $\mathbf{F}_{tar} \in \mathbb{R}^{C \times \frac{H}{s} \times \frac{W}{s}}$  ( $s$  is the scale factor) for the SR task.

### B. Multi-modal Transformer

Our multi-modal transformer fuses the different modalities, as shown in Fig. 3, which employs two symmetric branches,

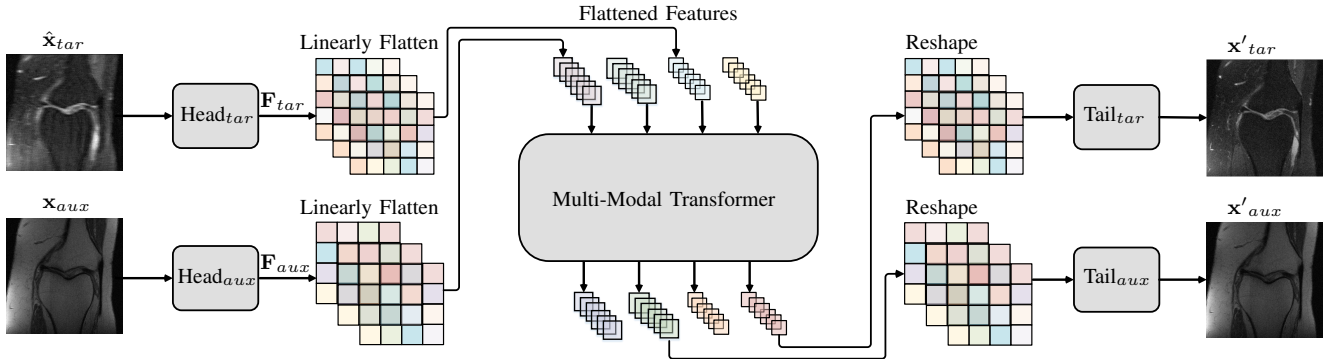


**Fig. 2:** An illustration of the proposed MTrans framework. Our architecture consists of two branches, *e.g.*, a target branch and an auxiliary branch. This in turn are each divided into three components: two **heads** for extracting modality-specific features of different scales from the multi-modal input images (*e.g.*, the fully sampled auxiliary modality image  $x_{aux}$  of large patch size with target zero filling  $\hat{x}_{tar}$  or the LR image  $\hat{x}_{tar}$ ); a **multi-modal transformer** for aggregating the different modalities; and two **tails** in the target modality for mapping the features into restored images.

*e.g.*, a target branch and an auxiliary branch. To handle 2D images, following [18], we split the features of the two modalities  $F_{aux}$  and  $F_{tar}$  into patches, which are regarded as sequences of "words". Specifically, we first reshape the features of the auxiliary modality  $F_{aux} \in \mathbb{R}^{C \times H \times W}$  into a sequence of patches  $F_{aux_i}^p \in \mathbb{R}^{P^2 \times C}, i = \{1, \dots, N\}$ , where  $N = \frac{HW}{P^2}$  is the number of patches or the length of the sequence for the transformer, and  $P$  is the resolution of each image patch. Similarly, we reshape the features of the target modality  $F_{tar} \in \mathbb{R}^{(P/2)^2 \times C}, i = \{1, \dots, N\}$ . Note that the resolution of the target image patch is half the size of the auxiliary modality. We use the different-sized image patches in the auxiliary and target modalities to produce stronger image features. Then, learnable position encodings  $E_{tar_i}^p \in \mathbb{R}^{(\frac{P}{2})^2 \times C}$  for the target branch and  $E_{aux_i}^p \in \mathbb{R}^{P^2 \times C}$  for the auxiliary modality are added to each branch to maintain the position information of each image patch [18], [19]:

$$\begin{aligned} \mathbf{z}_{tar}^0 &= [E_{tar_1}^p + F_{tar_1}^p, E_{tar_2}^p + F_{tar_2}^p, \dots, E_{tar_i}^p + F_{tar_i}^p], \\ \mathbf{z}_{aux}^0 &= [E_{aux_1}^p + F_{aux_1}^p, E_{aux_2}^p + F_{aux_2}^p, \dots, E_{aux_i}^p + F_{aux_i}^p], \end{aligned} \quad (1)$$

where  $\mathbf{z}_{tar}^0 \in \mathbb{R}^{(\frac{P}{2})^2 \times C}$  and  $\mathbf{z}_{aux}^0 \in \mathbb{R}^{P^2 \times C}$  are the position-embedded patches of the target and auxiliary modality, which are sent to a series of cascaded cross transformer encoder modules (see Fig. 3). Each cross transformer encoder consists of two components, *e.g.*, a cross transformer encoder<sub>tar</sub> for the target modality and cross transformer encoder<sub>aux</sub> for the auxiliary modality. Note that encoder<sub>tar</sub> fuses the features from the auxiliary modality, while encoder<sub>aux</sub> fuses the features from the target modality. Such a cross pattern ensures that each branch learns important information from the other modality. The green arrows in Fig. 3 correspond to information updating for the modality of the current branch, and the red arrows facilitate information exchange between the two modalities.

We can formulate our multi-modal transformer as:

$$[\mathbf{z}_{tar}^N, \mathbf{z}_{aux}^N] = \mathcal{M}^N([\mathbf{z}_{tar}^0, \mathbf{z}_{aux}^0]), \quad (2)$$

where  $\mathcal{M}^N$  is the multi-modal transformer module consisting of the  $N$ -th cross transformer encoder, and  $\mathbf{z}_{aux}^N \in \mathbb{R}^{P^2 \times C}$  and  $\mathbf{z}_{tar}^N \in \mathbb{R}^{(\frac{P}{2})^2 \times C}$  are the output sequences of the multi-modal transformer.

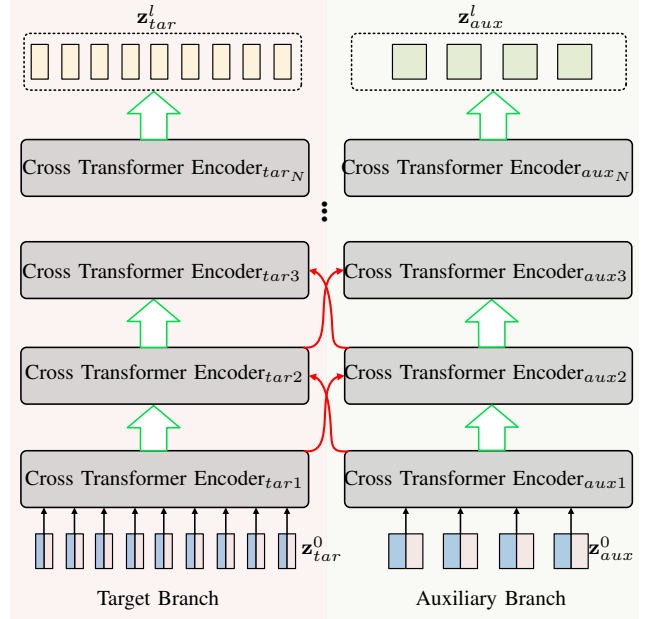


**Fig. 3:** Architecture of the **multi-modal transformer** for multi-modal feature fusion, which is a cascade of several **cross transformer encoder** modules. **Green** arrows correspond to information updates while **red** arrows facilitate information exchange between the two modalities.

1) **Cross Transformer Encoder:** Our cross transformer encoder aims to effectively fuse the two modalities. As shown in Fig. 4, the position-embedded patches  $\mathbf{z}_{tar}^0, \mathbf{z}_{aux}^0$  are first linearly projected (LP) to align their dimensions, which can be formulated as:

$$\begin{aligned} \mathbf{z}_{tar}^{lp} &= \text{LP}(\mathbf{z}_{tar}^0), \mathbf{z}_{tar}^{lp} \in \mathbb{R}^{P^2 \times C}, \\ \mathbf{z}_{aux}^{lp} &= \text{LP}(\mathbf{z}_{aux}^0), \mathbf{z}_{aux}^{lp} \in \mathbb{R}^{(\frac{P}{2})^2 \times C}, \end{aligned} \quad (3)$$

where  $\mathbf{z}_{tar}^{lp}$  and  $\mathbf{z}_{aux}^{lp}$  are the aligned features. These features are sent to the cross attention module with a layernorm and residual shortcut to fuse the two modalities, followed by a

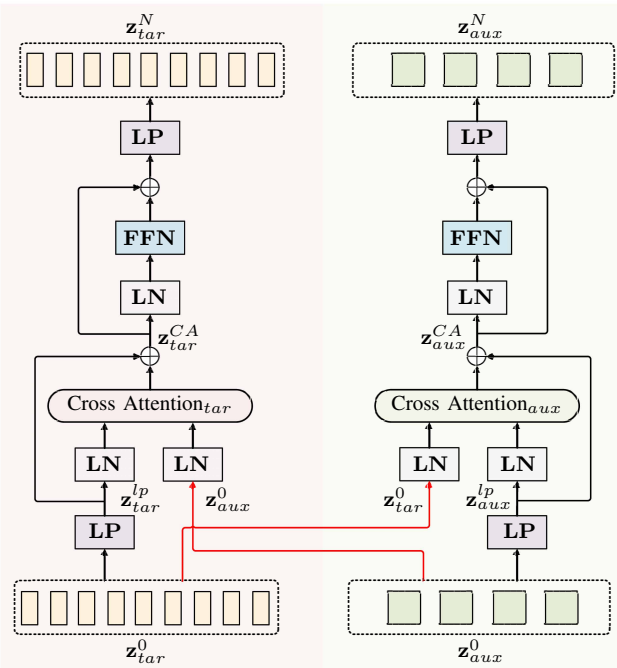


**Fig. 4:** An illustration of the **cross transformer encoder**. Our cross transformer encoder consists of cross attention<sub>tar</sub> and cross attention<sub>aux</sub> modules with different patch sizes, enabling it to produce stronger features for the restoration of the target modality. The red arrows facilitate information exchange between the two modalities.

feedforward network. This can be formulated as:

$$\begin{aligned} \mathbf{z}_{tar}^{CA} &= CA_{tar} \left( \text{LN} \left( \mathbf{z}_{tar}^{lp}, \mathbf{z}_{aux}^0 \right) \right) + \mathbf{z}_{tar}^0, \\ \mathbf{z}_{aux}^{CA} &= CA_{aux} \left( \text{LN} \left( \mathbf{z}_{tar}^0, \mathbf{z}_{aux}^{lp} \right) \right) + \mathbf{z}_{aux}^0, \\ \mathbf{z}_{tar}^i &= LP \left( \text{FFN} \left( \text{LN} \left( \mathbf{z}_{tar}^{CA} \right) \right) + \mathbf{z}_{tar}^{CA} \right), \\ \mathbf{z}_{aux}^i &= LP \left( \text{FFN} \left( \text{LN} \left( \mathbf{z}_{aux}^{CA} \right) \right) + \mathbf{z}_{aux}^{CA} \right), \end{aligned} \quad (4)$$

where  $i = [1, 2, \dots, N]$ , CA<sub>tar</sub> and CA<sub>aux</sub> are the cross attention modules for different modalities, and FFN denotes the feedforward network. LN denotes the layernorm, which is used for dimension alignment. The output sequence features  $\mathbf{z}_{aux}^i$  and  $\mathbf{z}_{tar}^i$  of the two branches are saved as the input of the next cross transformer encoder.

**2) Cross Attention Module:** Our cross attention module is an improved multi-head attention module which absorbs features from the auxiliary modality that contribute to the target modality. Specifically, in order to fuse the different modalities more efficiently and effectively, the features in the current branch serve as a query that interacts with the features from the other branch through attention. Note that the query features have already been dimensionally aligned with the features from the other branch. In other words, the feature sizes in the two branches are different. This allows our cross attention fusion module to learn both clear structural information and subtle pixel-level features. An illustration of our symmetric cross-attention module is shown in Fig. 5. For the target branch, we use the aligned features  $\mathbf{z}_{tar}^{lp}$  after layer normalization  $\text{LN}(\mathbf{z}_{tar}^{lp}) \in \mathbb{R}^{P^2 \times C}$  as the query (Q), and

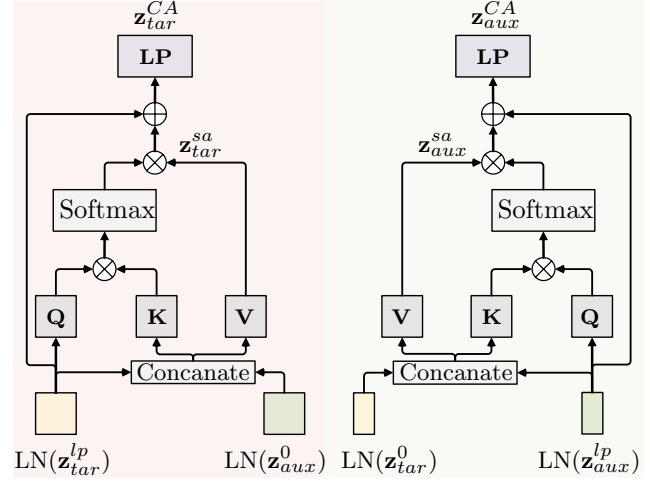


**Fig. 5:** **Cross attention module.** The features of the auxiliary branch are aligned with the target branch of large patch size, while the features of the target branch are aligned with the auxiliary branch of large patch size.

concatenate them with the features from the auxiliary branch  $\text{LN}(\mathbf{z}_{aux}^0) \in \mathbb{R}^{P^2 \times C}$  to serve as the key (K) and value (V). Similarly, for the auxiliary branch, the aligned features  $\mathbf{z}_{aux}^{lp}$  after layer normalization  $\text{LN}(\mathbf{z}_{aux}^{lp}) \in \mathbb{R}^{(\frac{P}{2})^2 \times C}$  serve as Q, and these are concatenated with the features from the target branch  $\text{LN}(\mathbf{z}_{tar}^0) \in \mathbb{R}^{(\frac{P}{2})^2 \times C}$  to serve as K and V. Then, the correspondence between the two modalities in each branch can be found using the following bilinear model:

$$\mathbf{z}^{sa} = \text{softmax} \left( \frac{\mathbf{Q} \mathbf{K}^T}{\sqrt{\mathbf{D}/h}} \right) \mathbf{V}, \quad (5)$$

where  $\mathbf{z}^{sa}$  is divided into  $\mathbf{z}_{tar}^{sa}$  for the target branch and  $\mathbf{z}_{aux}^{sa}$  for the auxiliary branch,  $\mathbf{D}$  is the embedding dimension and  $h$  is the number of heads in the cross attention mechanism. Finally, the outputs  $\mathbf{z}_{tar}^{CA}$  and  $\mathbf{z}_{aux}^{CA}$  of a cross attention module can be defined as follows:

$$\begin{aligned} \mathbf{z}_{tar}^{CA} &= LP(\mathbf{z}_{tar}^{sa} + \text{LN}(\mathbf{z}_{tar}^{lp})), \\ \mathbf{z}_{aux}^{CA} &= LP(\mathbf{z}_{aux}^{sa} + \text{LN}(\mathbf{z}_{aux}^{lp})). \end{aligned} \quad (6)$$

### C. Tails

Finally, the outputs of the multi-modal transformer encoder  $\mathbf{z}_{tar}^N$  and  $\mathbf{z}_{aux}^N$  are fed into two tail modules to predict the restored images, as:

$$\mathbf{x}'_{tar} = \text{Tail}_{tar}(\mathbf{z}_{tar}^N), \text{ and } \mathbf{x}'_{aux} = \text{Tail}_{aux}(\mathbf{z}_{aux}^N), \quad (7)$$

where the output  $\mathbf{x}'_{tar}$  is an image of size  $H \times W$  for both the reconstruction task and SR task.

### D. Loss

Following [48], [49], we simply use the  $L_1$  loss to evaluate our results:

$$L = \frac{1}{M} \sum_{m=1}^M \alpha \left\| \mathbf{x}'_{tar}^m - \mathbf{x}_{tar}^m \right\|_1 + (1-\alpha) \left\| \mathbf{x}'_{aux}^m - \mathbf{x}_{aux}^m \right\|_1, \quad (8)$$

where  $\alpha$  weights the trade-off between the two modalities, and  $M$  is the number of training samples.

## V. EXPERIMENTS

In this section, we first introduce the datasets and baselines used in our experiments, followed by the implementation details. Then, we summarize and analyze the experimental results. Finally, we conduct an ablation study to investigate the effectiveness of our multi-modal strategies.

### A. Datasets and Baselines

1) **Datasets:** We use two raw MR image datasets to evaluate our method: (1) **fastMRI** [50] is the largest open-access raw MR image dataset, officially provided at <https://fastmri.med.nyu.edu/>. Following [9], we filter out 227 and 24 pairs of PDWI and FS-PDWI knee volumes for training and validation. PDWIs are used to guide the restoration of the FS-PDWI modality. (2) **uiMRI** was collected using a 3T system (provided by United Imaging Healthcare uMR 790; informed written consent was obtained from all the subjects, and all experiments were carried out in accordance with the approved guidelines) with two different protocols (whole brain T1WI and T2WI  $k$ -space sampling) on 400 subjects. The slice thickness is 4 mm and matrix size is  $320 \times 320 \times 19$ . The uiMRI dataset is split subject-wise with a ratio of 7:1:2 for the training/validation/test sets, where T1WI is the auxiliary modality and T2WI is the target modality. All the experimental datasets are aligned through affine registration before our experiments.

2) **Performance Evaluation:** For quantitative study, peak signal-to-noise ratio (PSNR), structural similarity index (SSIM) and normalized mean square error (NMSE) are used to evaluate the performance of our method [50]. We compare our model with the following single- and multi-modal algorithms. Single-modal MR image reconstruction/SR methods: we evaluate the most popular SR method (EDSR) [51]; the most popular MR image reconstruction method, UNet, provided by fastMRI [50]; and a standard transformer framework for MR image reconstruction/SR (TransMRI). Multi-modal reconstruction/SR methods: we investigate a DenseUNet model for multi-modal MR image reconstruction called MDUNet [8]; a conditional GAN framework for multi-modal MR image reconstruction named rsGAN [15]; a non-progressive multi-modal MR image SR network called PRO [16]; and a deep CNN model for multi-modal MR image SR named MCSR [45]. All compared methods are retrained using their default settings. The various forms of our multi-modal fusion strategies will be discussed in the ablation studies. For the reconstruction task, we use the an equispaced undersampling pattern with  $8 \times$  acceleration for fastMRI, and a random pattern with  $6 \times$  acceleration for uiMRI. For the SR task, we use  $4 \times$  enlargement for both fastMRI and uiMRI to evaluate the effectiveness of our method.

### B. Implementation Details

Our model is implemented in PyTorch with four NVIDIA Tesla V100 GPUs and 32GB of memory per card. We use the SGD optimizer with a learning rate of 1e-4 and a mini-batch size of 8, and train our model over 50 epochs. The parameter

$\alpha$  is set to 0.9, the effectiveness of which is verified in the ablation studies. The number of cross attention heads is set to 4, and the number of channels  $C$  in the feature map generated by  $\text{Head}_{tar}$  and  $\text{Head}_{aux}$  is set to 16. We use  $N = 4$  cross transformer encoders in our network.

### C. Results on MR Image Reconstruction

1) **Quantitative Evaluation:** We evaluate our reconstruction results by computing the SSIM, PSNR, and NMSE between the restored image and the fully sampled ground truth image. In Table I, we show the results of our reconstruction over the two raw MR image datasets. The first row provides the single-modal MR image reconstruction methods, while the second row includes the CNN-based multi-modal methods and our multi-modal transformer model. From the results, we find that the PSNR and SSIM values of the single-modal UNet are relatively low, especially on the uiMRI dataset. Similarly, the results of the standard single-modal transformer framework TransMRI are lower than other multi-modal methods. However, with the help of the auxiliary modality, the PSNR, SSIM and NMSE of MDUNet and rsGAN are improved to a certain degree. Thus, we can conclude that the auxiliary modality is complementary to the target modality. Our MTrans achieves 29.3 dB in PSNR and 0.268 in SSIM on the fastMRI dataset, and improves the reconstruction results of multi-modal CNN methods from 30.7 dB to 31.7 dB on uiMRI.

2) **Qualitative Evaluation:** For qualitative analysis, we provide the reconstruction results on the uiMRI dataset in Fig. 6. The more obvious the structure in the blue error map, the worse the restoration. As can be seen, reconstructions with zero-filling produce significant aliasing artifacts and lose anatomical details. Columns 2-4 in Fig. 6 show the reconstruction results of single-modal methods. Compared with zero-filling, single-modal methods can somewhat improve the reconstruction. However, multi-modal methods (the last three methods in Fig. 6) provide even further improvements, as verified by their corresponding error maps. Notably, our method yields the lowest reconstruction error, better preserving important anatomical details.

### D. Results on MR image Super-Resolution

1) **Quantitative Evaluation:** We evaluate our MTrans with the competing baseline methods on the SR task in Table II. This table summarizes the  $4 \times$  enlargement results of all methods on the two raw MR image datasets. Similar to Table I, the first row shows the single-modal MR image SR methods, while the second row includes the CNN-based multi-modal methods as well as our multi-modal transformer model. As can be seen from the table, the SR results are similar to those obtained for reconstruction. Specifically, the single-modal architectures, whether based on CNNs or transformers, are not as effective as the multi-modal methods. However, the multi-modal CNN methods are not as effective as our model. For example, our method improves the PSNR result of the best multi-modal CNN method from 31.0 dB to 31.9 dB on the fastMRI dataset, while on the uiMRI dataset it increases it from 34.8 dB to

**TABLE I:** Average (with standard deviation) **reconstruction** results, in terms of SSIM, PSNR and NMSE, under different undersampling patterns. The best and second-best results are marked in **red** and **blue**, respectively.

fastMRI	Equispaced			uiMRI	Random		
	Method	SSIM↑	PSNR↑		Method	SSIM↑	PSNR↑
Zero-filling	0.442±0.10	24.5±1.37	0.057±0.05	Zero-filling	0.700±0.09	27.0±1.70	0.067±0.010
UNet	0.565±0.06	28.2±1.15	0.046±0.02	UNet	0.849±0.05	28.9±1.57	0.044±0.006
TransMRI	0.607±0.05	28.4±0.81	0.038±0.01	TransMRI	0.861±0.02	28.9±1.31	0.044±0.005
MDUNet	0.600±0.05	28.6±1.00	0.040±0.01	MDUNet	0.900±0.03	30.0±1.53	0.034±0.006
rsGAN	<b>0.608±0.04</b>	<b>28.9±1.03</b>	<b>0.033±0.02</b>	rsGAN	<b>0.908±0.03</b>	<b>30.7±1.46</b>	<b>0.028±0.005</b>
<b>MTrans</b>	<b>0.638±0.03</b>	<b>29.3±0.89</b>	<b>0.030±0.01</b>	<b>MTrans</b>	<b>0.931±0.02</b>	<b>31.7±1.33</b>	<b>0.024±0.004</b>

**TABLE II:** Average (with standard deviation) **super-resolution** results, in terms of SSIM, PSNR and NMSE, under different datasets. The best and second-best results are marked in **red** and **blue**, respectively.

fastMRI	4×			uiMRI	4×		
	Method	SSIM↑	PSNR↑		Method	SSIM↑	PSNR↑
Bicubic	0.400±0.07	16.9±1.70	0.917±0.06	Bicubic	0.526±0.05	8.3±1.20	0.900±0.030
EDSR	0.580±0.04	28.1±1.64	0.045±0.04	EDSR	0.941±0.07	32.3±1.04	0.012±0.004
TransMRI	0.600±0.03	29.9±1.44	0.048±0.02	TransMRI	0.940±0.04	33.5±1.17	0.009±0.005
PRO	0.700±0.02	30.8±1.60	0.038±0.03	PRO	<b>0.945±0.07</b>	34.4±0.97	0.007±0.003
MCSR	<b>0.704±0.03</b>	<b>31.0±1.31</b>	<b>0.033±0.03</b>	MCSR	0.944±0.07	<b>34.8±0.97</b>	<b>0.006±0.003</b>
<b>MTrans</b>	<b>0.719±0.02</b>	<b>31.9±1.19</b>	<b>0.031±0.02</b>	<b>MTrans</b>	<b>0.959±0.05</b>	<b>36.1±0.99</b>	<b>0.005±0.003</b>

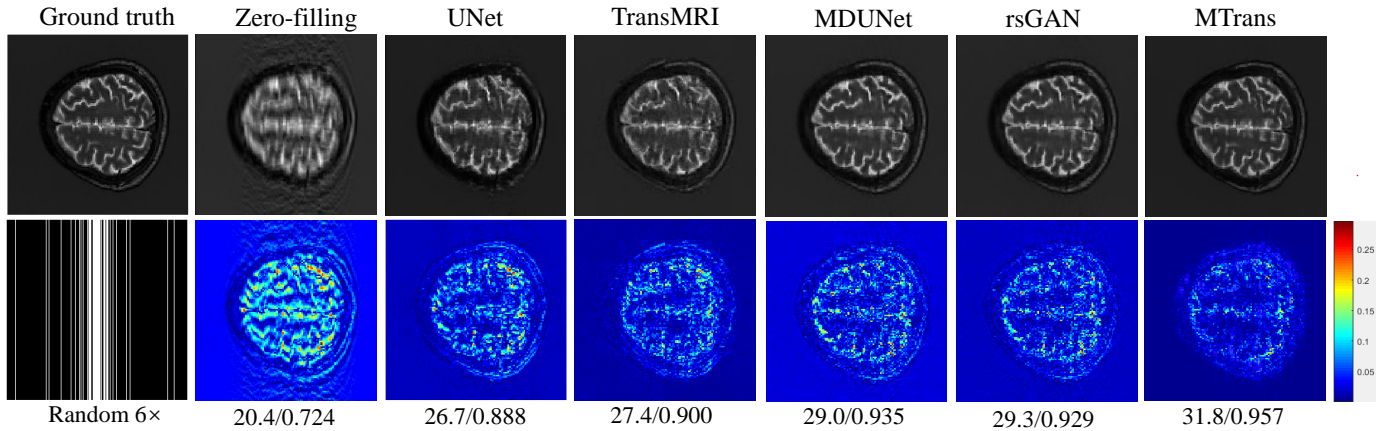


**Fig. 6:** Comparison of different methods in terms of reconstruction results on the uiMRI dataset. Reconstructed images and error maps are presented with corresponding quantitative measurements in PSNR/SSIM. The more obvious errors, the worse the restoration results. The first three methods represent the single-modal results, while the last three represent the multi-modal results.

36.1 dB. These results further confirm the effectiveness of our multi-modal approach.

Fig. 7 shows the 4× enlargement of target modality images from fastMRI. The first two rows show the images restored by the single-modal methods, while the last two provide show the results of the multi-modal methods. From this figure, we can see that the basic structure of the image can be restored by single-modal methods (*e.g.*, EDSR and TransMRI). However, the methods based on multi-modal fusion significantly improve the results, with smaller errors and clearer structures. In particular, our MTrans produces high-quality images with clear details, minimal checkerboard effects, and less structural loss. Further, our method can effectively restore the entire structure of the knee. This superior performance is attributed

to the fact that our MTrans can effectively aggregate MR image information from different modalities to obtain stronger features.

### E. Ablation Studies

In this section, we first investigate the effectiveness of our approach by comparing it with different fusion strategies. Then, we analyze the trade-off effects between the two modalities.

1) *Comparison of Different Fusion Schemes*: To evaluate the effectiveness of the key components in our model, we study two models in the ablation study. The first is a multi-modal transformer with early fusion, named ETransMRI, where the different modalities are fused as input. The second is our

**TABLE III:** Ablation study (with standard deviation) of reconstruction results on the two datasets. The best and second-best results are marked in **red** and **blue**, respectively.

Method	fastMRI			uiMRI		
	SSIM↑	PSNR↑	NMSE↓	SSIM↑	PSNR↑	NMSE↓
ETransMRI	0.619±0.03	29.0±1.10	0.037±0.01	0.915±0.02	30.5±1.43	0.030±0.004
ITransMRI	<b>0.622±0.03</b>	<b>29.2±0.90</b>	<b>0.038±0.02</b>	<b>0.920±0.03</b>	<b>31.0±1.21</b>	<b>0.028±0.005</b>
<b>MTrans</b>	<b>0.628±0.03</b>	<b>29.3±0.89</b>	<b>0.035±0.01</b>	<b>0.931±0.02</b>	<b>31.7±1.33</b>	<b>0.024±0.004</b>

**TABLE IV:** Ablation study (with standard deviation) of SR results on the two datasets. The best and second-best results are marked in **red** and **blue**, respectively.

Method	fastMRI			uiMRI		
	SSIM↑	PSNR↑	NMSE↓	SSIM↑	PSNR↑	NMSE↓
ETransMRI	0.668±0.02	31.0±1.21	0.037±0.02	0.953±0.05	35.6±1.09	0.006±0.002
ITransMRI	<b>0.698±0.03</b>	<b>31.0±1.10</b>	<b>0.034±0.03</b>	<b>0.942±0.06</b>	<b>35.8±1.02</b>	<b>0.006±0.004</b>
<b>MTrans</b>	<b>0.719±0.02</b>	<b>31.9±1.19</b>	<b>0.031±0.02</b>	<b>0.959±0.05</b>	<b>36.1±0.99</b>	<b>0.005±0.003</b>

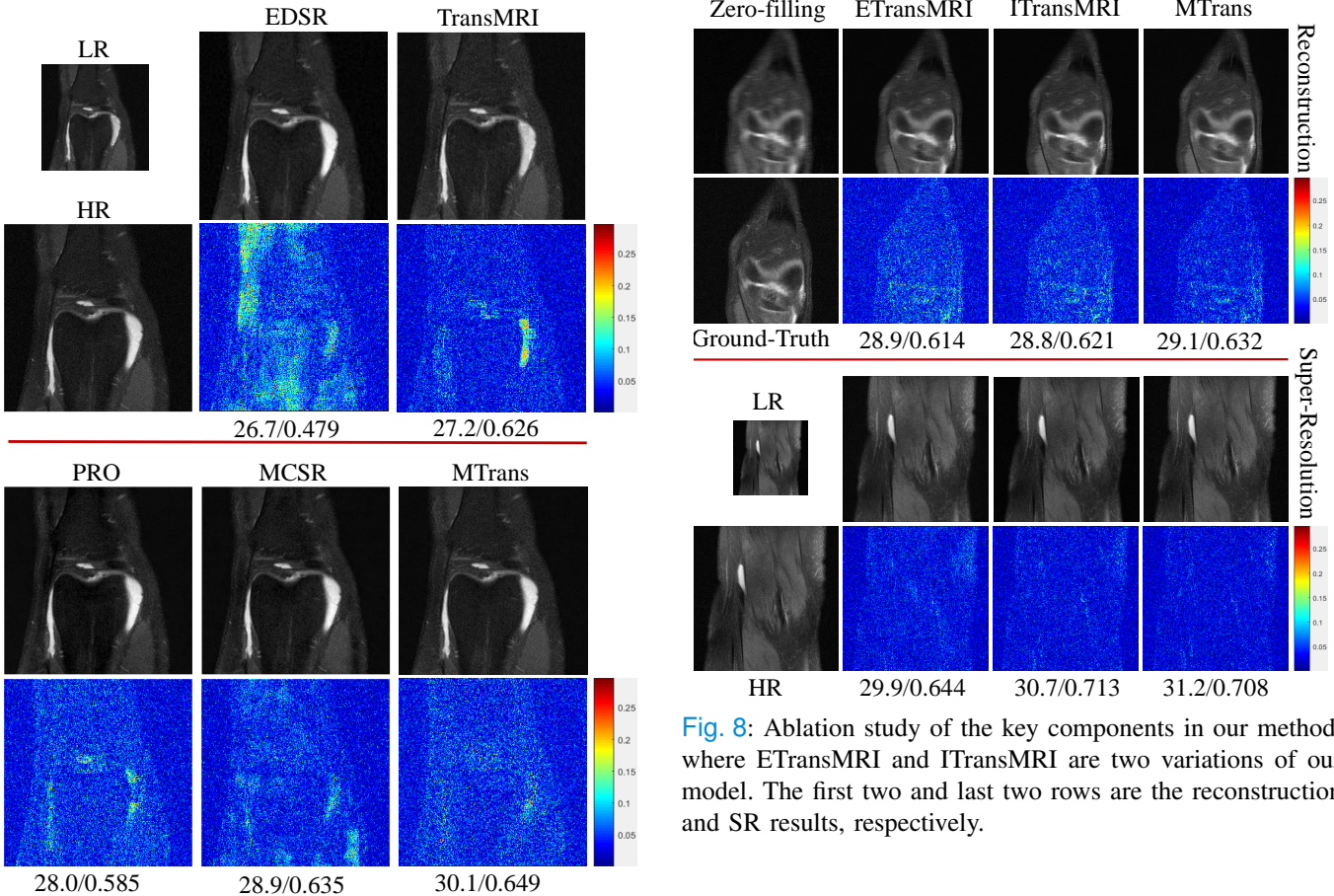


**Fig. 7:** Comparison of different methods in terms of SR results on the fastMRI dataset. SR images and error maps are presented with corresponding quantitative measurements in PSNR/SSIM. The more obvious the errors, the worse the restoration results. The first two rows show the single-modal results, while the last two rows provide the multi-modal results.

cross multi-modal transformer with same-scale fusion, named

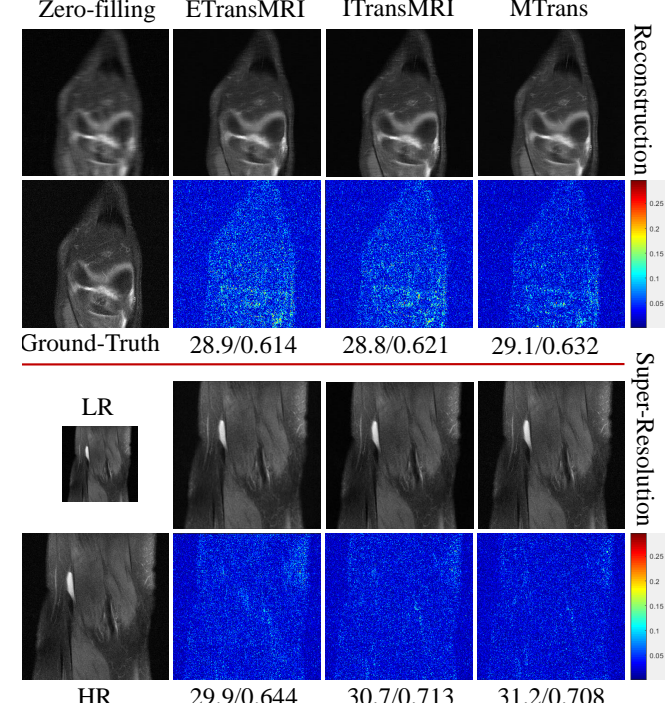


**Fig. 8:** Ablation study of the key components in our method, where ETransMRI and ITransMRI are two variations of our model. The first two and last two rows are the reconstruction and SR results, respectively.

ITransMRI. We summarize the reconstruction and SR results on fastMRI and uiMRI in Table III and Table IV, respectively. As can be seen, ETransMRI obtains the worst performance, which supports our conclusion that feature-level fusion can provide richer supplementary information than simple fusion. Since early fusion does not learn information at the feature level, it is not the most effective strategy for accelerating multi-modal MR imaging. In addition, because the fusion method of ITransMRI is too monotonous, and different-scale information cannot be extracted between the two different modalities,

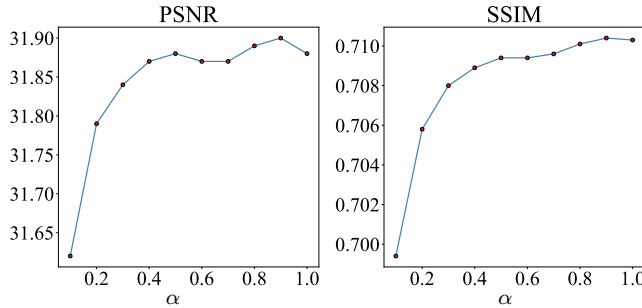


**Fig. 9:** Analysis of trade-off ( $\alpha$ ) between the two modalities in terms of PSNR and SSIM. The greater the value of  $\alpha$ , the greater the influence of the target modality, and the smaller the influence of the auxiliary modality.

the restoration of ITransMRI is not optimal. In contrast, our MTrans inherits the fusion information of different modalities at multiple scales, enhances the fusion features, and captures both the obvious structural information and subtle pixel-level features. The results in this section also demonstrate its strong ability to mine key information for guiding the target modality.

To qualitatively analyze the different fusion schemes, we show visual results on fastMRI with error maps in Fig. 8. The first two are the reconstruction results, while the last two rows are the SR results. From this figure, we can see that both ITransMRI and ETransMRI can effectively restore the image. However, MTrans achieves the lowest texture error, and provides results that are almost as clear as the ground truth. This indicates that our cross attention in the multi-modal transformer is effective for accelerating multi-modal MR imaging in both reconstruction and super-resolution.

**2) Effect of Trade-Off Between the Two Modalities:** We next investigate the influence of  $\alpha$ , which weights the trade-off between the two modalities. Specifically, the ratio  $\alpha$  determines the weights of both the target and auxiliary branches. The greater the value of  $\alpha$ , the greater the influence of the target modality, and the smaller the influence of the auxiliary modality. We record the SR results of our method on fastMRI in Fig. 9. As can be seen, our model achieves the best PSNR and SSIM scores at  $\alpha = 0.9$ . When  $\alpha = 1$ , the PSNR performance quickly degrades, while the SSIM degrades only slightly. This is likely because the auxiliary modality is fused with the ground truth at multiple scales, so the weight of the auxiliary branch loss is not affected very much.

## VI. CONCLUSION

In this work, we focus on exploring rich global knowledge in image for accelerated multi-modal MR imaging. For this purpose, we proposed a universal transformer framework, named MTrans, for accelerated multi-modal MR imaging, which can be used for MR image reconstruction and SR to effectively restore the target modality under the guidance of the auxiliary modality. By fusing the feature maps of different modalities, the proposed MTrans is helpful to learn the global information of multi-modal MR image, obtaining higher quality reconstructed images and significantly reduce artifacts. In particular, the proposed cross attention module can

explore the fusion strategy in different scales, to both obtain clear structural information and subtle pixel-level information. We conducted extensive experiments on the fastMRI and real-world clinical datasets under different settings of undersampling patterns. The results demonstrated our model against outperforms state-of-the-art methods in accelerated MR imaging. This work provides promising guidelines for further research into multi-modal MR imaging with transformers.

## REFERENCES

- [1] Y. Zhang, Z. Dong, P. Phillips, S. Wang, G. Ji, and J. Yang, “Exponential wavelet iterative shrinkage thresholding algorithm for compressed sensing magnetic resonance imaging,” *Information Sciences*, vol. 322, pp. 115–132, 2015.
- [2] Y. Chen, T. Xiao, C. Li, Q. Liu, and S. Wang, “Model-based convolutional de-aliasing network learning for parallel mr imaging,” in *International Conference on Medical Image Computing and Computer-Assisted Intervention*. Springer, 2019, pp. 30–38.
- [3] H. K. Aggarwal, M. P. Mani, and M. Jacob, “Modl: Model-based deep learning architecture for inverse problems,” *IEEE transactions on medical imaging*, vol. 38, no. 2, pp. 394–405, 2018.
- [4] G. Wang, J. C. Ye, and B. De Man, “Deep learning for tomographic image reconstruction,” *Nature Machine Intelligence*, vol. 2, no. 12, pp. 737–748, dec 2020. [Online]. Available: <http://www.nature.com/articles/s42256-020-00273-z>
- [5] Y. Chen, Y. Xie, Z. Zhou, F. Shi, A. G. Christodoulou, and D. Li, “Brain mri super resolution using 3d deep densely connected neural networks,” in *2018 IEEE 15th International Symposium on Biomedical Imaging (ISBI 2018)*. IEEE, 2018, pp. 739–742.
- [6] A. S. Chaudhari, Z. Fang, F. Kogan, J. Wood, K. J. Stevens, E. K. Gibbons, J. H. Lee, G. E. Gold, and B. A. Hargreaves, “Super-resolution musculoskeletal mri using deep learning,” *Magnetic resonance in medicine*, vol. 80, no. 5, pp. 2139–2154, 2018.
- [7] S. McDonagh, B. Hou, A. Alansary, O. Oktay, K. Kamnitsas, M. Rutherford, J. V. Hajnal, and B. Kainz, “Context-sensitive super-resolution for fast fetal magnetic resonance imaging,” in *Molecular Imaging, Reconstruction and Analysis of Moving Body Organs, and Stroke Imaging and Treatment*. Springer, 2017, pp. 116–126.
- [8] L. Xiang, Y. Chen, W. Chang, Y. Zhan, W. Lin, Q. Wang, and D. Shen, “Deep-learning-based multi-modal fusion for fast mr reconstruction,” *IEEE Transactions on Biomedical Engineering*, vol. 66, no. 7, pp. 2105–2114, 2018.
- [9] K. Xuan, S. Sun, Z. Xue, Q. Wang, and S. Liao, “Learning mri k-space subsampling pattern using progressive weight pruning,” in *International Conference on Medical Image Computing and Computer-Assisted Intervention*. Springer, 2020, pp. 178–187.
- [10] W. Chen, J. Zhao, Y. Wen, B. Xie, X. Zhou, L. Guo, L. Yang, J. Wang, Y. Dai, and D. Zhou, “Accuracy of 3-t mri using susceptibility-weighted imaging to detect meniscal tears of the knee,” *Knee Surgery, Sports Traumatology, Arthroscopy*, vol. 23, no. 1, pp. 198–204, 2015.
- [11] B. Bilgic, V. K. Goyal, and E. Adalsteinsson, “Multi-contrast reconstruction with bayesian compressed sensing,” *Magnetic resonance in medicine*, vol. 66, no. 6, pp. 1601–1615, 2011.
- [12] P. Song, L. Weizman, J. F. Mota, Y. C. Eldar, and M. R. Rodrigues, “Coupled dictionary learning for multi-contrast mri reconstruction,” *IEEE transactions on medical imaging*, vol. 39, no. 3, pp. 621–633, 2019.
- [13] Z. Lai, X. Qu, H. Lu, X. Peng, D. Guo, Y. Yang, G. Guo, and Z. Chen, “Sparse mri reconstruction using multi-contrast image guided graph representation,” *Magnetic resonance imaging*, vol. 43, pp. 95–104, 2017.
- [14] L. Sun, Z. Fan, X. Fu, Y. Huang, X. Ding, and J. Paisley, “A deep information sharing network for multi-contrast compressed sensing mri reconstruction,” *IEEE Transactions on Image Processing*, vol. 28, no. 12, pp. 6141–6153, 2019.
- [15] S. U. Dar, M. Yurt, M. Shahdloo, M. E. Ildiz, B. Tinaz, and T. Çukur, “Prior-guided image reconstruction for accelerated multi-contrast mri via generative adversarial networks,” *IEEE Journal of Selected Topics in Signal Processing*, vol. 14, no. 6, pp. 1072–1087, 2020.
- [16] Q. Lyu, H. Shan, C. Steber, C. Helis, C. T. Whitlow, M. Chan, and G. Wang, “Multi-contrast super-resolution mri through a progressive network,” *IEEE Transactions on Medical Imaging*, 2020.
- [17] S. Khan, M. Naseer, M. Hayat, S. W. Zamir, F. S. Khan, and M. Shah, “Transformers in Vision: A Survey,” *arXiv*, jan 2021. [Online]. Available: <http://arxiv.org/abs/2101.01169>

[18] A. Dosovitskiy, L. Beyer, A. Kolesnikov, D. Weissenborn, X. Zhai, T. Unterthiner, M. Dehghani, M. Minderer, G. Heigold, S. Gelly *et al.*, “An image is worth 16x16 words: Transformers for image recognition at scale,” *arXiv preprint arXiv:2010.11929*, 2020.

[19] N. Carion, F. Massa, G. Synnaeve, N. Usunier, A. Kirillov, and S. Zagoruyko, “End-to-end object detection with transformers,” in *European Conference on Computer Vision*. Springer, 2020, pp. 213–229.

[20] J. Chen, Y. Lu, Q. Yu, X. Luo, E. Adeli, Y. Wang, L. Lu, A. L. Yuille, and Y. Zhou, “Transunet: Transformers make strong encoders for medical image segmentation,” *arXiv preprint arXiv:2102.04306*, 2021.

[21] W. Wang, C. Chen, M. Ding, J. Li, H. Yu, and S. Zha, “Transbts: Multimodal brain tumor segmentation using transformer,” *arXiv preprint arXiv:2103.04430*, 2021.

[22] J. P. Haldar, D. Hernando, and Z.-P. Liang, “Compressed-sensing mri with random encoding,” *IEEE transactions on Medical Imaging*, vol. 30, no. 4, pp. 893–903, 2010.

[23] Y. Shi, Y. Gao, Y. Zhang, J. Sun, X. Mou, and Z. Liang, “Spectral ct reconstruction via low-rank representation and region-specific texture preserving markov random field regularization,” *IEEE Transactions on Medical Imaging*, 2020.

[24] A. Pramanik, H. Aggarwal, and M. Jacob, “Deep generalization of structured low-rank algorithms (deep-slr),” *IEEE Transactions on Medical Imaging*, 2020.

[25] J. P. Haldar and J. Zhuo, “P-loraks: low-rank modeling of local k-space neighborhoods with parallel imaging data,” *Magnetic resonance in medicine*, vol. 75, no. 4, pp. 1499–1514, 2016.

[26] J. He, Q. Liu, A. G. Christodoulou, C. Ma, F. Lam, and Z.-P. Liang, “Accelerated high-dimensional mr imaging with sparse sampling using low-rank tensors,” *IEEE transactions on medical imaging*, vol. 35, no. 9, pp. 2119–2129, 2016.

[27] K. K. Bhatia, A. N. Price, W. Shi, J. V. Hajnal, and D. Rueckert, “Super-resolution reconstruction of cardiac mri using coupled dictionary learning,” in *2014 IEEE 11th International Symposium on Biomedical Imaging (ISBI)*. IEEE, 2014, pp. 947–950.

[28] Q. Liu, Q. Yang, H. Cheng, S. Wang, M. Zhang, and D. Liang, “Highly undersampled magnetic resonance imaging reconstruction using autoencoding priors,” *Magnetic resonance in medicine*, vol. 83, no. 1, pp. 322–336, 2020.

[29] S. Wang, Z. Su, L. Ying, X. Peng, S. Zhu, F. Liang, D. Feng, and D. Liang, “Accelerating magnetic resonance imaging via deep learning,” in *2016 IEEE 13th International Symposium on Biomedical Imaging (ISBI)*. IEEE, 2016, pp. 514–517.

[30] Y. Yang, J. Sun, H. Li, and Z. Xu, “Admm-csnet: A deep learning approach for image compressive sensing,” *IEEE Trans. Pattern Anal. Mach. Intell.*, vol. 42, no. 3, pp. 521–538, 2020.

[31] S. Wang, Z. Su, L. Ying, X. Peng, S. Zhu, F. Liang, D. Feng, and D. Liang, “Accelerating magnetic resonance imaging via deep learning,” *IEEE International Symposium on Biomedical Imaging*, pp. 514–517, 2016.

[32] K. H. Jin, M. T. McCann, E. Froustey, and M. Unser, “Deep convolutional neural network for inverse problems in imaging,” *IEEE Trans. Image Process.*, vol. 26, no. 9, pp. 4509–4522, 2017.

[33] Y. Chen, Y. Xie, Z. Zhou, F. Shi, A. G. Christodoulou, and D. Li, “Brain mri super resolution using 3d deep densely connected neural networks,” in *2018 IEEE 15th International Symposium on Biomedical Imaging (ISBI 2018)*. IEEE, 2018, pp. 739–742.

[34] B. Zhu, J. Z. Liu, S. F. Cauley, B. R. Rosen, and M. S. Rosen, “Image reconstruction by domain-transform manifold learning,” *Nature*, vol. 555, no. 7697, pp. 487–492, 2018.

[35] D. Lee, J. Yoo, S. Tak, and J. C. Ye, “Deep residual learning for accelerated mri using magnitude and phase networks,” *IEEE Transactions on Biomedical Engineering*, vol. 65, no. 9, pp. 1985–1995, 2018.

[36] C.-M. Feng, Z. Yang, G. Chen, Y. Xu, and L. Shao, “Dual-octave convolution for accelerated parallel mr image reconstruction,” in *Proceedings of the 35th AAAI Conference on Artificial Intelligence (AAAI)*, 2021.

[37] C.-M. Feng, Z. Yang, H. Fu, Y. Xu, J. Yang, and L. Shao, “Donet: Dual-octave network for fast mr image reconstruction,” in *IEEE Transactions on Neural Networks and Learning Systems*, 2021.

[38] T. M. Quan, T. Nguyen-Duc, and W.-K. Jeong, “Compressed sensing mri reconstruction using a generative adversarial network with a cyclic loss,” *IEEE Trans. on Medical Imaging*, vol. 37, no. 6, pp. 1488–1497, 2018.

[39] G. Yang, S. Yu, H. Dong, G. Slabaugh, P. L. Dragotti, X. Ye, F. Liu, S. Arridge, J. Keegan, Y. Guo *et al.*, “Dagan: Deep de-aliasing generative adversarial networks for fast compressed sensing mri reconstruction,” *IEEE Trans. on Medical Imaging*, vol. 37, no. 6, pp. 1310–1321, 2017.

[40] M. Mardani, E. Gong, J. Y. Cheng, S. S. Vasanawala, G. Zaharchuk, L. Xing, and J. M. Pauly, “Deep generative adversarial neural networks for compressive sensing mri,” *IEEE Trans. on Medical Imaging*, vol. 38, no. 1, pp. 167–179, 2018.

[41] Q. Lyu, C. You, H. Shan, and G. Wang, “Super-resolution mri through deep learning,” *arXiv preprint arXiv:1810.06776*, 2018.

[42] J. Schlemper, J. Caballero, J. V. Hajnal, A. N. Price, and D. Rueckert, “A deep cascade of convolutional neural networks for dynamic mr image reconstruction,” *IEEE Trans. on Medical Imaging*, vol. 37, no. 2, pp. 491–503, 2017.

[43] H. Zheng, F. Fang, and G. Zhang, “Cascaded dilated dense network with two-step data consistency for mri reconstruction,” in *Adv. Neural Inform. Process. Syst.*, 2019, pp. 1744–1754.

[44] T. Eo, Y. Jun, T. Kim, J. Jang, H.-J. Lee, and D. Hwang, “Kiki-net: cross-domain convolutional neural networks for reconstructing undersampled magnetic resonance images,” *Magnetic resonance in medicine*, vol. 80, no. 5, pp. 2188–2201, 2018.

[45] K. Zeng, H. Zheng, C. Cai, Y. Yang, K. Zhang, and Z. Chen, “Simultaneous single-and multi-contrast super-resolution for brain mri images based on a convolutional neural network,” *Computers in biology and medicine*, vol. 99, pp. 133–141, 2018.

[46] T. Zhou, H. Fu, G. Chen, J. Shen, and L. Shao, “Hi-net: hybrid-fusion network for multi-modal mr image synthesis,” *IEEE Trans. on Medical Imaging*, 2020.

[47] C.-H. Pham, A. Ducournau, R. Fablet, and F. Rousseau, “Brain mri super-resolution using deep 3d convolutional networks,” in *2017 IEEE 14th International Symposium on Biomedical Imaging (ISBI 2017)*. IEEE, 2017, pp. 197–200.

[48] A. Sriram, J. Zbontar, T. Murrell, C. L. Zitnick, A. Defazio, and D. K. Sodickson, “Grappanet: Combining parallel imaging with deep learning for multi-coil mri reconstruction,” in *IEEE Conf. Comput. Vis. Pattern Recog.*, 2020, pp. 14315–14322.

[49] S. Wang, H. Cheng, L. Ying, T. Xiao, Z. Ke, H. Zheng, and D. Liang, “Deepcomplexmri: Exploiting deep residual network for fast parallel mr imaging with complex convolution,” *Magnetic Resonance Imaging*, vol. 68, pp. 136–147, 2020.

[50] J. Zbontar, F. Knoll, A. Sriram, M. J. Muckley, M. Bruno, A. Defazio, M. Parente, K. J. Geras, J. Katsnelson, H. Chandarana *et al.*, “fastmri: An open dataset and benchmarks for accelerated mri,” *arXiv preprint arXiv:1811.08839*, 2018.

[51] B. Lim, S. Son, H. Kim, S. Nah, and K. Mu Lee, “Enhanced deep residual networks for single image super-resolution,” in *Proceedings of the IEEE conference on computer vision and pattern recognition workshops*, 2017, pp. 136–144.